
Investigating Stateful Defenses Against Black-Box Adversarial Examples

Ryan Feng^{*1}, Ashish Hooda^{*2}, Neal Mangaokar^{*1}, Kassem Fawaz², Somesh Jha²,
Atul Prakash¹

¹ University of Michigan, Ann Arbor, ² University of Wisconsin, Madison

¹{rtfeng, nealmgkr, aprakash}@umich.edu,

²{ahooda, kfawaz, jha}@cs.wisc.edu

* denotes equal contribution

Abstract

Defending machine-learning (ML) models against white-box adversarial attacks has proven to be extremely difficult. Instead, recent work has proposed *stateful defenses* in an attempt to defend against a more restricted black-box attacker. These defenses operate by tracking a history of incoming model queries, and rejecting those that are suspiciously similar. The current state-of-the-art stateful defense Blacklight was proposed at USENIX Security '22 and claims to prevent nearly 100% of attacks on both the CIFAR10 and ImageNet datasets. In this paper, we observe that an attacker can significantly reduce the accuracy of a Blacklight-protected classifier (e.g., from 82.2% to 6.4% on CIFAR10) by simply adjusting the parameters of an existing black-box attack. Motivated by this surprising observation, since existing attacks were evaluated by the Blacklight authors, we provide a systematization of stateful defenses to understand why existing stateful defense models fail. Finally, we propose a stronger evaluation strategy for stateful defenses comprised of adaptive score and hard-label based black-box attacks. We use these attacks to successfully reduce even reconfigured versions of Blacklight to as low as 0% robust accuracy.

1 Introduction

Machine learning (ML) models for tasks such as audio and image classification are known to be vulnerable to adversarial examples. Adversarial examples are imperceptibly modified inputs that are misclassified by the model, and pose a significant threat to the deployment of ML models for applications such as deepfake detection [34], autonomous driving [19, 27], medical image classification [21, 40], or identity verification [37]. When an attacker has full access to a model (white-box access), defenses have been elusive. Even in a high-dimensional search space, an attacker can usually find adversarial examples using gradient-based attacks [3, 7, 14, 17, 20, 29, 38].

An alternative threat model is black-box access, where an attacker has only query access to a model via an API exposed by a Machine-Learning-as-a-Service (MLaaS) platform [1, 2, 13]. The model returns label probabilities or labels, but the attacker is not assumed to have further access to the model or its training data. Unfortunately, such models can still be successfully attacked using gradient or boundary estimation techniques to construct adversarial examples [6, 9, 18, 23, 26, 30, 31, 41, 42]. These estimation techniques involve multiple queries on nearby inputs to approximate the local loss landscape.

One recent line of work that attempts to defend against black-box attacks are *stateful defenses*. Observing that standard attacks must sample many close-by points for gradient/boundary estimation, these defenses use an internal state to track queries and reject those that are deemed “too similar”

by a content-similarity engine. The first such defense was proposed by Chen et al. [11], who argued that such defenses may offer defenders the much-needed advantage against attackers in realistic black-box settings. They claimed significant improvements in robustness by using a per-account state and banning users who issue suspicious queries — an attacker would need to create hundreds of accounts on the service to get around similarity checks, thereby raising the attack cost. In this paper, we refer to this defense as the Original Stateful Defense (OSD). A more recent defense called Blacklight [27] was proposed at USENIX Security ’22 to overcome two key limitations of OSD [11]. First, Blacklight observed that an adversary could easily create new Sybil [15, 43] accounts to find attacks, and thus replaces the per-account state with a global state to prevent the attacker from making progress on other accounts. Second, Blacklight also replaced OSD’s content similarity engine with a hash-based approach to improve scalability. Blacklight claims near 100% robustness against a broad range of query-based black-box attacks.

In this work, we revisit these stateful defenses, in particular Blacklight, which has shown considerable promise and is the state-of-the-art stateful defense to our knowledge. Our first contribution is to show that we can significantly reduce the robust accuracy of Blacklight from 82.2% to 6.4% on CIFAR10, and from 73.0% to 28.0% on ImageNet by using different hyperparameter settings for the existing, standard NES attack [23] (which was considered by the Blacklight authors in its original setting). OSD’s robustness can be similarly reduced with fewer attacker accounts. See Section 2.5 for details.

Motivated by this somewhat surprising finding, given that OSD and Blacklight were thoroughly evaluated against a range of attacks in their original papers (including NES), our second contribution is a systematization of stateful defenses to better understand when they may or may not work. To do this, we introduce a general framework from which both OSD and Blacklight can be instantiated as special cases (see Section 2). The components of the framework include a feature extractor, which defines the space on which similarity is detected, and the action module, which identifies collisions based on a similarity threshold and defines behavior when a collision is detected (banning accounts/rejection in the case of OSD and Blacklight).

We then use this framework to identify two potential limitations of Blacklight as originally presented. First, we observe that there exists an inherent trade-off between similar-query detection and natural accuracy. The similarity threshold provides a way to manage this trade-off, i.e., sacrificing natural accuracy to detect more attack queries. We thus consider and re-evaluate multiple threshold settings for Blacklight to better analyze this trade-off. Second, we consider the possibility that the hash-based feature extractor used for the content similarity engine in Blacklight may be a factor in the success of the attack. We thus also re-evaluate Blacklight using additional hash-based feature extractors, including the popular NeuralHash [5]. We find that, depending on the dataset, these changes can improve Blacklight’s resistance to NES attacks. For example, simply increasing the 0-to-1 similarity threshold from 0.5 (original paper) to 0.7 boosts CIFAR10 robust accuracy from 6.8% to 68% under the NES attack that uses more effective hyperparameter values. Additionally, ImageNet appears to resist attacks even more than CIFAR10 if a neural hash extractor is used, suggesting that the choice of feature extractor used for the content similarity engine is a critical component in a stateful defense. See Section 3 for details.

Our third and final contribution is to propose a stronger adaptive attack methodology for a broad class of stateful defenses including OSD, Blacklight, and the more robust variations of Blacklight we identified that utilize a higher threshold or a different feature extractor (see Section 4). Specifically, we introduce two attacks that modify existing black-box attacks to be stronger against stateful defenses: NESRadial and BoundaryRadial. These adaptive attacks aim to construct adversarial examples by *evading the content-similarity engine employed by the stateful defense*. At a high level, NESRadial proceeds by adaptively estimating the thresholding parameter of the similarity engine via a simple binary-search protocol. It then submits queries just outside of this threshold to estimate attack gradients with traditional NES techniques [23, 41]. Likewise, BoundaryRadial also attempts to improve on the hard-label Boundary [6] attack to evade detection by using a similar evading strategy. These new attacks further degrade the accuracy of robust variations of Blacklight significantly; for instance, even for a similarity threshold of 0.7, adversarial accuracy drops to 0% for CIFAR-10 under the BoundaryRadial attack and to 8% for ImageNet under the NESRadial attack.

Summary: We provide a systematized analysis of stateful defenses through the use of a general framework to abstract existing approaches. This analysis exposes limitations of existing stateful

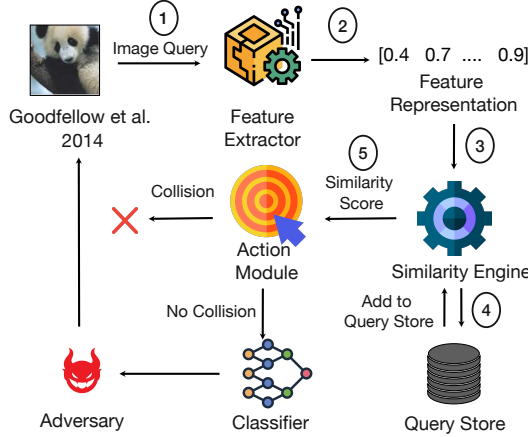


Figure 1: Our general stateful defense framework pipeline. Given an input query, we first run the image through the feature extractor. We then pass the output feature representation to the similarity engine, which compares this representation with those in the query store and outputs a similarity score. The action module then decides whether it is a collision or not. If it is not a collision, we query the model, add it to the query store, and return the output. If it is a collision, the action depends on the specific implementation details of the action module.

defenses. Building on these limitations, we provide a stronger attack evaluation pipeline comprising two adaptive attacks — NESRadial and BoundaryRadial — that significantly reduce the robustness of existing stateful defenses.

2 Characterizing Stateful Defenses

We begin by developing a general framework for stateful defenses. We first identify and provide definitions for key defense components and then describe how existing defense proposals can be seen as simple instantiations of this framework.

2.1 Notation

Vectors are denoted in boldface. Let \mathcal{D} be the distribution over input space $\mathcal{X} \times \mathcal{Y}$, where $\mathcal{X} \in \mathbb{R}^n$ is the space of n -dimensional images, and \mathcal{Y} is the class label space. Here, $\mathcal{D}_{\mathcal{X}}$ and $\mathcal{D}_{\mathcal{Y}}$ are the respective marginal distributions on \mathcal{D} . Let $F : \mathcal{X} \rightarrow \mathbb{R}^{|\mathcal{Y}|}$ be the “soft-label” DNN classifier trained using loss function L that outputs probabilities over the classes, i.e., $F(\mathbf{x})_i$ is the probability that $\mathbf{x} \in \mathcal{X}$ belongs to the i^{th} class. The “hard-label” classifier can then be given by $f(\mathbf{x}) = \arg \max_i F(\mathbf{x})_i$. Given image $\mathbf{x} \in \mathcal{X}$ with true label $y \in \mathcal{Y}$, and a perturbation budget ϵ , an adversarial example is any image \mathbf{x}^* such that $f(\mathbf{x}^*) \neq y$ and $\|\mathbf{x}^* - \mathbf{x}\| \leq \epsilon$.

2.2 The Stateful Defense Model

The key intuition behind stateful defenses is that query-based black-box attacks need to query “similar” images in order to estimate gradients. Therefore, rejecting any query that is similar to a historically queried image should prevent these attacks. To analyze these defenses, we observe that a generic stateful defense model can be broken down into six major components: *classifier*, *feature extractor*, *query store*, *similarity engine*, and *action module*.

Classifier. The model is a DNN classifier function F (see Section 2.1) to be protected against query-based black-box attacks.

Feature Extractor. The feature extractor is a function $h(\cdot)$ that extracts a representation of incoming queries, such that queries can be compared in the space induced by h , e.g., the neural encoder in OSD [11] or Pixel-SHA, the SHA-256 based probabilistic hash in Blacklight [27]. Queries are compared with the given distance function, which is a metric $d(\cdot, \cdot)$ over the space induced by

h . As an example, for two queries \mathbf{x}_1 and \mathbf{x}_2 , the defense d computes their similarity score as $d(h(\mathbf{x}_1), h(\mathbf{x}_2))$

Query Store. The query store is a finite-capacity stateful buffer Q that stores a history of incoming queries. Specifically, given an incoming query \mathbf{x} , $h(\mathbf{x})$ is inserted into the store. Optionally, the defense could choose to only insert $h(\mathbf{x})$ into the store if it did not collide with anything previously in the store. The store can either be global (as in Blacklight), or account-specific, i.e., one per user (as in OSD).

Similarity Engine. The similarity engine s is used to compute the distance of a given query from the most similar element(s) in the store. Specifically, given an incoming query \mathbf{x} and query store Q , s returns a single scalar similarity score that represents the distance from the “closest” store entries. For example, given a hash function, a similarity engine could compute the Hamming distance between \mathbf{x} and its nearest neighbor(s).

Action Module. The action module action is a function that identifies when collisions occur, and takes the necessary steps to prevent attacks from progressing. Specifically, given a scalar similarity score s returned by the search function, the action module observes a collision if $a(s) \leq \tau$, where τ is a distance threshold. If a collision is observed, the action invokes some defensive behavior, e.g., banning the user account like OSD [11] or rejecting the query like in Blacklight [27].

Defenses are assumed to be hosted by a web-based Machine-Learning-as-a-Service (MLaaS) platform. Examples of such platforms include Clarifai [13], Amazon Rekognition [2], and Automatic License Plate Recognition systems [1]. Users can submit queries by registering an account with the service, and interfacing with a public API.

A stateful defense model (SDM) can thus be described by its components as a 6-tuple $\text{SDM}(f, h, d, Q, a, \tau, \text{action})$. When a user submits query \mathbf{x} via the API, the stateful defense executes the algorithmic workflow summarized in Figure 1. At a high level, this workflow is a search algorithm over the (global or account-specific) query store(s), and operates in two steps. *First*, the similarity engine computes the similarity score (in the feature space) between \mathbf{x} and the closest entry in the store(s). *Second*, this score is compared to threshold τ — if it is below the threshold, the defense considers \mathbf{x} to have induced a collision, and the defensive behavior is triggered. If not, the new query is inserted in the store, and the defense defers to the underlying classifier f for a standard response.

2.3 Attacker Threat Model

Our work focuses on stateful defenses against black-box adversarial examples. Without loss of generality, for evaluation, we focus on the image classification domain as in prior work on stateful defenses. Our attacker model is similar to that followed by prior work on stateful defenses [11, 27]. Specifically, we consider an attacker with black-box query access to the SDM. We consider the strongest attacker under the black-box model that is fully aware of the choice of h , and any possible associated parameters. However, as per Kerchoff’s principle, we also allow the SDM to keep a single private key, e.g., a private salt for hash function implementations of h such as those used by Blacklight. Armed with this knowledge, the attacker has a query budget of B queries which can be used to achieve misclassification. Specifically, given image \mathbf{x} with label y , the attacker, with a given query budget, aims to construct an adversarial example, i.e., image \mathbf{x}^* such that:

$$f(\mathbf{x}^*) \neq y \quad \text{and} \quad \|\mathbf{x} - \mathbf{x}^*\| \leq \epsilon$$

Finally, we allow the attacker to create unlimited accounts (e.g., Sybil accounts [15, 43]) to send their queries where necessary.

2.4 Existing Defenses

Prior work has proposed two stateful defenses: the Original Stateful Defense (OSD) [11], and Blacklight [27]. In this section, we demonstrate how both defenses can be reduced to simple instantiations of our framework. A summary can be found in Table 1.

OSD. Originally proposed by Chen et al. [11], OSD employs a neural similarity encoder as the feature extractor h . The encoder outputs a sub d -dimensional embedding vector, and is trained using a contrastive loss [4]. The contrastive loss encourages perceptually similar images, (e.g.,

Defense	Query Store	Feature Extractor	Similarity Engine	Action
OSD [11]	Per Account	Neural Encoder	k NN over ℓ_2 Distance ($k = 50$)	Ban Account
Blacklight [27]	Global	Pixel-SHA	k NN over Hamming Distance ($k = 1$)	Reject Query

Table 1: Existing defenses OSD and Blacklight can be expressed in terms of their choices for each framework component.

an image and the corresponding rotated image) to have nearby embeddings by ℓ_2 distances. The embeddings of queries are stored in an account-specific query store. To detect whether incoming query \mathbf{x} induces a collision, OSD uses a similarity engine s that computes the average ℓ_2 distance between $h(x)$ and its k -nearest neighbors in the store. Finally, if a collision is detected, OSD’s action module action bans the user’s account.

Blacklight. Blacklight [27] was proposed to address two immediate limitations of OSD: (1) the run-time complexity of OSD’s similarity engine is $O(|Q|)$, and (2) simply banning accounts becomes less effective in the face of Sybil accounts [15, 43], since a persistent attacker can simply acquire a large number of new accounts and continue their normal attack procedure.

To address the first limitation, Blacklight proposes Pixel-SHA, a probabilistic hash function as its feature extractor h . Specifically, given input \mathbf{x} , the probabilistic hash function quantizes the image by quantization factor q :

$$\mathbf{x}_q = \frac{\mathbf{x} \bmod 255}{q} \quad (1)$$

and then hashes multiple segments of w pixels at strides of size p ¹, as given by:

$$\{\mathbf{x}_q^i, \mathbf{x}_q^{i+w}\} \forall 0 < i < q \quad \text{s.t. } i \bmod p = 0 \quad (2)$$

The top 50 of these hashes are concatenated as the final output of h . Since the output of h is a hash, Blacklight employs approximate nearest-neighbor search over normalized Hamming distances (which range between 0 and 1) in its similarity engine s , which can be computed in $O(1)$ time.

To address the second limitation, Blacklight employs a global hash-table as its query store. Since the store is global, collisions are detected regardless of the number of accounts created by the attacker. Finally, Blacklight’s action module chooses to reject queries, i.e., deny classification service when a collision is detected.

Blacklight assumes that the global store is large but finite and needs to be reset infrequently, say, once a day to handle the query workload. An attacker can pause to issue subsequent queries till a reset so as to evade Blacklight’s similarity check. With a reset of once per day however, Blacklight authors report that it would take an attacker approximately 3 years to do the fastest successful attack, which is a significant slowdown in an attacker’s capabilities.

2.5 Breaking Existing Defenses

The current state-of-the-art defense, Blacklight [27], claims significant robustness against existing black-box query-based attacks, reducing them to near-zero success rates. Robustness is measured using the standard robust accuracy metric:

$$R(f) = \mathbb{E}_{(\mathbf{x}, y) \sim \mathcal{D}} \left[\max_{\|\mathbf{x} - \mathbf{x}^*\| \leq \epsilon} \mathbb{1}_{\{f(\mathbf{x}^*) = y\}} \right]$$

where ϵ is the attacker’s perturbation budget.

Our first key observation is that Blacklight’s robustness is *significantly overestimated*. It suffers from significant drops in robust accuracy under an adjusted version of the popular query-efficient black-box attack called Natural Evolutionary Strategies (NES) [23]. Below we present a brief overview of NES, and how we configure it to break Blacklight.

¹Quantizing the image aims to eliminate most small changes introduced by the attack. In other words, for appropriately large values of q , Blacklight hopes that attack queries largely quantize to the same values.

Dataset	Defense	Natural	NES ($\sigma = 0.05$)	NES ($\sigma = 0.01$)	NES ($\sigma = 0.001$)
CIFAR10	OSD [11]	91.7%	5.6% (1.7% / 1.2K)	6.6% (1.6% / 0.2K)	15.6% (1.6% / 0.2K)
	Blacklight [27]	91.7%	6.8% (0.6% / 1.2K)	6.4% (2.4% / 0.3K)	82.2% (95.6% / 0.1K)
ImageNet	Blacklight [27]	78.3%	50.0% (0.9% / 0.8K)	28.0% (0.8% / 1.4K)	73.0% (95.6% / 0.1K)

Table 2: *Takeaway: we find that different variances for NES can significantly lower accuracy than originally claimed.* We report the accuracy, average attack collision rate, and average attack query count when running the standard NES attack against existing defenses OSD [11] and Blacklight [27]. Lower accuracy implies the attack was more successful. NES is run with the original configuration of $\sigma = 0.001$ (as evaluated when originally proposed), as well as with two larger variances. Defenses are run under their officially recommended settings (Blacklight with $\tau = 0.5$, and OSD with $\tau = 2.75$). Collision rate and query count are averaged over successful attacks. We evaluate for 500 images on CIFAR10 and 100 images on ImageNet.

NES Attack Overview. The NES attack is a score-based attack that aims to construct adversarial examples by estimating the loss gradient. Given an image \mathbf{x} with true label y , NES iteratively operates in two stages. First, gradients are estimated for loss function L using finite differences over samples from a Gaussian distribution:

$$\nabla_x^{est} L = \mathbb{E}_{u \sim \mathcal{N}(0, I)} \left[\frac{1}{\sigma} L(x + \sigma u, y) u \right] \quad (3)$$

where σ^2 is the variance of the distribution.

Second, \mathbf{x} is moved with a step-size of η in the direction of this estimated gradient (i.e., via projected gradient descent) to increase the loss:

$$\mathbf{x}^{t+1} = \text{Proj}_{\mathbf{x} + \mathcal{S}}(\mathbf{x}^t + \eta \cdot \text{sgn}(\nabla_x^{est} L)) \quad (4)$$

where $\mathcal{S} = \{\delta : \|\delta\| \leq \epsilon\}$ and Proj is the projection operator. This process is repeated until the increase in loss elicits misclassification.

Experimental Setup. In this section, we evaluate OSD [11] and Blacklight [27] under their original settings on a ResNet-20 [22] classifier for CIFAR10 [25] and a ResNet-152 [22] classifier for ImageNet [35]. We test against NES attack [23] with three different variances: $\sigma = 0.05$, $\sigma = 0.01$, and $\sigma = 0.001$ (Blacklight evaluated with $\sigma = 0.001$). We use 64 directions for gradient estimation, an ℓ_∞ perturbation bound of 0.05, and a step-size of $\eta = 0.01$. We set the maximum number of steps to 200, which corresponds to a query budget of about 13K queries. We only evaluate OSD against CIFAR10, as the original paper did not evaluate on ImageNet and as such we do not have a neural encoder for ImageNet. For OSD, we use a threshold of $\tau = 2.75$, which is approximately the 0.1% false positive rate targeted by the original paper. Blacklight’s Pixel-SHA is configured with the parameters described in Section 2.4 using the default Blacklight recommendations, chosen by the authors after exhaustive search: $w = 20$ (CIFAR10), $w = 50$ (ImageNet), $q = 50$, $p = 1$, and an additive salt to prevent reverse-engineering.

Robustness against NES. Results are presented in Table 2. We find that while Blacklight [27] is robust to the smallest variance of 0.001, achieving robust accuracies of 82.2% and 73.0% on CIFAR10 and ImageNet, we find that its *robust accuracy drops below that of a random-guessing classifier when attack variance is increased*. Specifically, with $\sigma = 0.01$, the robust accuracy on Blacklight drops to 6.4% on CIFAR10 and 28.0% on ImageNet. The results with $\sigma = 0.05$ show that the amount we can increase σ is bounded, as those robust accuracies are higher than on $\sigma = 0.01$. We also see that the average query-store collision rate for successful attacks is much lower for $\sigma = 0.01$ than $\sigma = 0.001$.

For comparison, results of attacking OSD [11] with the same configurations are presented in row 1. OSD also expectedly breaks, since its only deterrent is to ban the user’s account (in which case the attacker simply creates a new account). However, we find that we can break OSD on the order of 10’s of accounts rather than the 100’s or 1000’s of accounts reported in the original paper.

3 Understanding the Limitations of Existing SDMs

SDM's are designed to be an effective solution for defending against black-box attacks. However, in Section 2.5, we found existing defenses to be less robust than previously thought, breaking under different configurations of the NES attack. More specifically, these defenses appear vulnerable to minor adjustments of the variance used during gradient estimation. This suggests that a more detailed analysis is needed to understand their limitations and to identify ways to potentially improve their effectiveness. Our analysis led us to identify alternative reconfigurations of these SDMs that may lead to increased robustness.

3.1 Large Variance Queries Evoke Existing SDMs

With no direct access to classifier parameters, black-box attacks approximate the model's loss landscape by making "similar" queries. Particularly, score-based black-box attacks such as NES [23] typically estimate the gradient of the model output over a Gaussian distribution:

$$\nabla_{\mathbf{x}} L = \mathbb{E}_{u \sim \mathcal{N}(0, \sigma^2)} [L(x + u)] \quad (5)$$

In fact, it can be shown that the choice of variance (σ^2) of the Gaussian samples influences the quality of the gradient estimate, i.e., quality is lower for larger variances:

Theorem 3.1. *Let $\mathbf{x} \in \mathbf{R}^d$ be an image query, $\nabla_{\mathbf{x}}$ be the true gradient for classifier loss L , and $g_1, \dots, g_k \in \mathbf{R}^d$ be k Gaussian vectors of variance σ^2 . Then, the norm of estimated gradient $G\nabla_{\mathbf{x}}$ (where G is a matrix of rows g_1, \dots, g_k) is bounded in probability by:*

$$\begin{aligned} \mathbf{P}[(1 - \delta) \|\nabla_{\mathbf{x}}\| \leq \|G\nabla_{\mathbf{x}}\| \leq (1 + \delta) \|\nabla_{\mathbf{x}}\|] &\geq \\ 1 - 2 \cdot \exp\left(-k - \frac{1 + \delta}{2\sigma^2}\right) \end{aligned}$$

where $0 \leq \delta \leq 1$ is the estimation error.

A detailed proof of this result can be found in Appendix A.0.1. The left-hand side represents the probability that our estimated gradient is "good", i.e., produces the same increase in loss as the true gradient. As σ increases, the lower bound on this probability decreases (right-hand side), suggesting that the estimate is less likely to produce the same increase in loss.

An SDM($f, h, d, Q, a, \tau, \text{action}$) aims to thwart the adversary's attempt to estimate the gradients by detecting similar queries and executing its action. Particularly, after the SDM answers query \mathbf{x} , it should detect all subsequent queries $\mathbf{x} + u$. The detection rate against these attack queries would then be denoted by :

$$\alpha^{det} = \mathbb{P}_{u \sim \mathcal{N}(0, \sigma^2)} [d(h(\mathbf{x} + u), h(\mathbf{x})) < \tau] \quad (6)$$

From Equation 6, we can see that the detection rate depends on the feature extractor h . For an ideal SDM, the detection rate α^{det} should be large even for larger σ , otherwise an adversary can just increase σ to evade detection. Unfortunately, we find that this is not the case for Blacklight's Pixel-SHA or OSD's neural extractors.

We observe this empirically in Figure 3, which plots the detection rate vs. variance for CIFAR10 and ImageNet. Furthermore, since SOTA for neural feature extractors has considerably improved since the release of OSD, and since no neural extractor is available for OSD on ImageNet, we trained new extractors for both datasets using Google's neural contrastive learning SimCLR framework [36]². For both Pixel-SHA and the neural extractors, regardless of threshold τ , Figure 3 indicates that α^{det} decreases with increase in variance σ . Interestingly, the neural extractor exhibits higher detection rates than Pixel-SHA for ImageNet.

3.2 Attack Detection is at Odds With Natural Performance

The natural accuracy of an SDM depends on the underlying classifier as well as the contents of the query store. Specifically, let α^{fp} be the false positive rate of the SDM, given by:

²Architecture and training details can be found in Section 5.1.

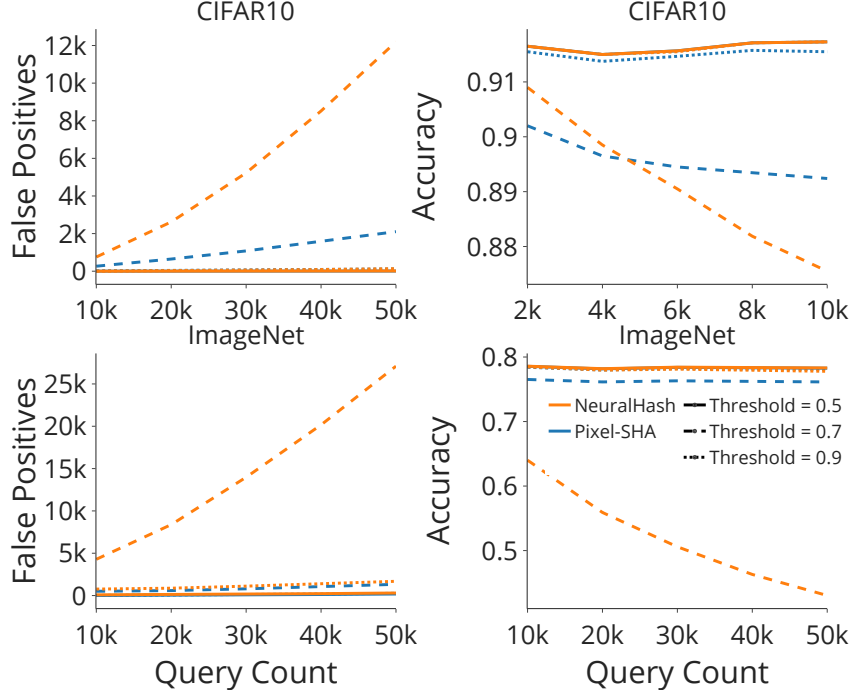


Figure 2: Number of false positives vs. query count (left), and accuracy vs. query count (right) for Blacklight’s Pixel-SHA, and updated versions of OSD’s neural extractor. Plots are presented at different normalized hamming distance thresholds $\in [0.5, 0.7, 0.9]$. Threshold values larger than 0.7, i.e., 0.9 tend to yield many false positives and low accuracy.

$$\alpha^{fp} = \mathbb{P}_{\mathbf{v} \sim \mathcal{D}_x} [d(h(\mathbf{v}), h(\mathbf{x})) < \tau] \quad (7)$$

Then, for a query store of size N , the SDM’s accuracy Acc is given by :

$$Acc = (1 - \alpha^{fp})^N \mathbb{P}_{(x,y) \sim \mathcal{D}} [f(x) = y] \quad (8)$$

It can be seen from Equation 8 that Acc degrades as a function of α^{fp} exponentially in the size of the query store. Modern services such as Facebook can service hundreds of millions of image queries per day [8] — thus, for an ideal SDM, $\alpha^{fp} \approx 0$ so that Acc is not influenced by benign usage. As per Equation 7, the natural solution to achieving this would be to decrease threshold τ . However, this suggests a trade-off between natural accuracy and attack detection, since the SDM must detect attack queries even at large variance, which calls for a larger τ (as per Equation 6 and Figure 3). In other words, the threshold τ provides a way to balance the trade-off and can be tuned to improve one at expense of the other.

3.3 Bounding the Trade-off between Attack Detection and False Positives

As discussed in Section 3.2, threshold τ provides a way to balance the trade-off between attack detection and false positive rates — increasing the threshold improves attack detection but increases the false positive rate, and vice versa. However, an ideal SDM needs both a high attack detection rate and a low false positive rate. In this section, we analyze the limits of this trade-off and provide upper bounds for the performance of a SDM.

Given $SDM(f, h, d, Q, a, \tau, \text{action})$ for data distribution \mathcal{D} , consider $h : \mathcal{X} \rightarrow \mathcal{H}$ to be a feature extractor that maps from the metric space $(\mathcal{X}, \hat{\ell}_2)$ to (\mathcal{H}, d) . Here we define (1) the n -dimensional input space $\mathcal{X} \in [0, 1]^n$, (2) $\hat{\ell}_2$ as the normalized euclidean distance and, (3) $d : \mathcal{H} \times \mathcal{H} \rightarrow [0, 1]$ as the distance metric defined on the feature space \mathcal{H} . As per work on metric spaces [28], we define

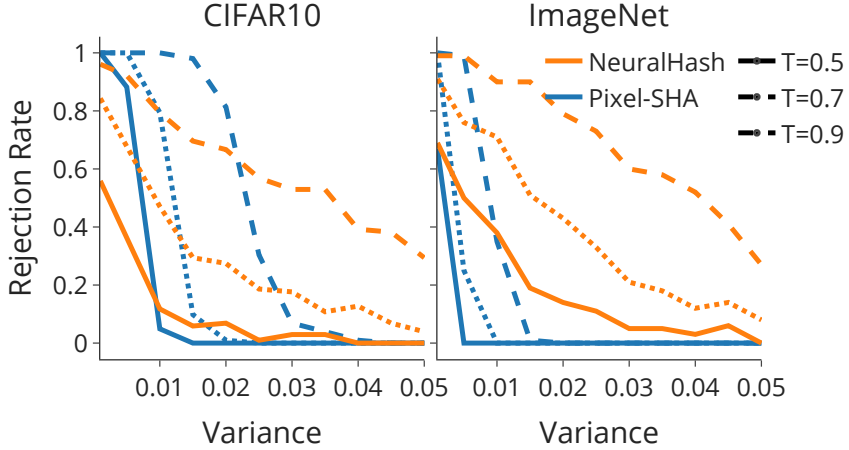


Figure 3: Rejection rate vs. attack query variance for Blacklight’s Pixel-SHA, and updated versions of OSD’s neural extractor. Plots are presented at different normalized hamming distance thresholds $\in [0.5, 0.7, 0.9]$ As variance increases, both feature extractors are unable to detect and reject queries.

Dataset	Defense	Natural	NES ($\sigma = 0.05$)	NES ($\sigma = 0.01$)	NES ($\sigma = 0.005$)
CIFAR10	BL ($h = \text{Pixel-SHA}$, $\tau = 0.5$)	91.7%	6.8% (0.6% / 1.2K)	6.4% (2.4% / 0.3K)	70.4% (89.4% / 0.4K)
	BL ($h = \text{Pixel-SHA}$, $\tau = 0.7$)	91.6%	68.0% (1.3% / 0.1K)	76.8% (90.8% / 3.4K)	80.0% (99.9% / 3.3K)
	BL ($h = \text{Neural}$, $\tau = 0.7$)	91.7%	60.8% (51.6% / 2.8K)	75.0% (91.2% / 5.5K)	76.4% (93.3% / 3.3K)
ImageNet	BL ($h = \text{Pixel-SHA}$, $\tau = 0.5$)	78.3%	50.0% (0.9% / 0.8K)	28.0% (0.8% / 1.4K)	23.0% (0.8% / 1.0K)
	BL ($h = \text{Pixel-SHA}$, $\tau = 0.7$)	78.1%	48.0% (0.9% / 1.1K)	31.0% (0.8% / 1.3K)	37.0% (28.7% / 0.6K)
	BL ($h = \text{Neural}$, $\tau = 0.7$)	77.7%	68.0% (78.4% / 2.5K)	75.0% (96.9% / 7.9K)	72.0% (98.8% / 6.3K)

Table 3: *Takeaway: we find that NES is less successful against these SDM reconfigurations, leaving room for improvement with a stronger attack.* We report the accuracy, average attack collision rate, and average attack query count when running the standard NES attack against the reconfigured SDMs in Section 3.4. Lower accuracy implies the attack was more successful. NES is run with $\sigma = 0.05$, $\sigma = 0.01$, and $\sigma = 0.005$. We include results for the original Blacklight [27] baseline ($h = \text{Pixel-SHA}$, $\tau = 0.5$), Blacklight with a higher threshold of 0.7, and Blacklight with NeuralHash as described in Section 3.4. Collision rate and query count are averaged over successful attacks. We evaluate for 500 images on CIFAR10 and 100 images on ImageNet.

the expansion and contraction properties of h to be:

$$\text{expansion}(h) : E_h = \max_{\mathbf{x}, \mathbf{y} \in \mathcal{X}} \frac{d(h(\mathbf{x}), h(\mathbf{y}))}{\frac{\|\mathbf{x} - \mathbf{y}\|_2}{\sqrt{n}}} \quad (9)$$

$$\text{contraction}(h) : C_h = \max_{\mathbf{x}, \mathbf{y} \in \mathcal{X}} \frac{\frac{\|\mathbf{x} - \mathbf{y}\|_2}{\sqrt{n}}}{d(h(\mathbf{x}), h(\mathbf{y}))} \quad (10)$$

We again define the attack detection and false positive rates over the marginal data distribution $\mathcal{D}_{\mathcal{X}}$ as

$$\alpha^{det} = \mathbb{P}_{\mathbf{x} \sim \mathcal{D}_{\mathcal{X}}, \mathbf{u} \sim \mathcal{N}(0, \sigma^2)} [d(h(\mathbf{x} + \mathbf{u}), h(\mathbf{x})) < \tau] \quad (11)$$

$$\alpha^{fp} = \mathbb{P}_{\mathbf{v}, \mathbf{x} \sim \mathcal{D}_{\mathcal{X}}} [d(h(\mathbf{v}), h(\mathbf{x})) < \tau] \quad (12)$$

Theorem 3.2. *Given the above setting, an SDM($f, h, d, Q, a, \tau, \text{action}$) cannot arbitrarily improve both - increase the attack detection rate (α^{det}) and decrease the false positive rate (α^{fp}). This trade-off is upper bounded by the expansion (E_h) and contraction (C_h) of the feature extractor, and the average normalized ℓ_2 distance between images in the marginal input distribution $\mathcal{D}_{\mathcal{X}}$, given by :*

$$\alpha^{det} (1 - n\alpha^{fp}) \leq \left(\frac{\sqrt{e} M_{\mathcal{D}_{\mathcal{X}}} E_h C_h}{\sigma} \right)^n \quad (13)$$

where, $M_{\mathcal{D}_{\mathcal{X}}} = \frac{1}{\sqrt{n}} \mathbb{E}_{\mathbf{v}, \mathbf{x} \sim \mathcal{D}_{\mathcal{X}}} [\|\mathbf{v} - \mathbf{x}\|_2]$ and e is the Euler’s number.

The proof is in Appendix B. In summary, the trade-off faces an upper bound that is independent of τ , i.e., there is an optimal τ beyond which the trade-off cannot be improved.

Furthermore, the RHS of Equation 13 also suggests that upper bound on the trade-off is likely to be larger if (1) the feature extractor (h) has both high expansion and contraction, (2) the average ℓ_2 distance between images in the marginal input distribution \mathcal{D}_X is large, i.e., images are “well spaced out”, and (3) the underlying model (f) cannot be attacked with queries of large variance σ^2 . Therefore, the feature extractor needs to compress attack queries close together (high C as per Equation 10), and expand natural queries to be far apart (high E as per Equation 9). Further, the SDM performs well if attack queries are “similar” to each other, and natural queries are not. Finally, if the underlying model can only be attacked using low variance queries, they will be detected by the defense.

3.4 Reconfiguring SDMs

In this section, we use our findings in Section 3 to guide two reconfigurations of SDMs.

For our first reconfiguration, *we simply consider Blacklight with a larger threshold*. This choice was guided by observations presented in Figure 2, which plots the natural accuracy for Pixel-SHA at various normalized hamming distance thresholds of 0.5 (default), 0.7, and 0.9 (where normalized hamming distance ranges between 0 and 1). We observe that the default threshold of 0.5 used by Blacklight can safely be raised to 0.7 without significantly affecting natural accuracy, i.e., drops of $< 0.1\%$ for CIFAR10 and $< 0.2\%$ for ImageNet. Further increase to 0.9 significantly degrades accuracy. From Figure 3, we can also see that both the Pixel-SHA and neural extractors detect more attack queries at a threshold of 0.7 as compared to 0.5. We term this configuration BL (h = Pixel-SHA, τ = 0.7).

For our second reconfiguration, *we consider Blacklight with neural hash extractors instead of Pixel-SHA*. Blacklight employs a global query store (instead of per-account stores) and rejects queries (instead of banning) which solves multiple limitations of OSD [27]. However, our findings in Section 3.1 indicate that (up-to-date versions of) OSD’s neural extractor detects more attack queries without decreasing the natural accuracy as compared to Pixel-SHA. We additionally improve the practicality of neural embeddings by converting them to hashes, so that we can retain the $O(1)$ efficiency of Blacklight’s content similarity engine (kNN over normalized Hamming distance). To this end, we run standard locality-sensitive hashing using a uniformly sampled random projection matrix on the embeddings output by the extractor so that the output is a hash. Finally, we again set the threshold to 0.7 following Figure 2, and term this configuration BL (h = Neural, τ = 0.7).

Robustness of reconfigurations against NES. Given that BL (h = Pixel-SHA, τ = 0.7) and BL (h = Neural, τ = 0.7) were reconfigured for improved robustness, we now re-evaluate them against the standard NES attack that successfully reduced the accuracy of standard Blacklight (which we now refer to as BL (h = Pixel-SHA, τ = 0.5)). Table 3 presents robust accuracy of both configurations under the same experimental settings used in Section 2.5. We observe that both configurations indeed offer improved robustness against vanilla NES, even at higher variance settings. Furthermore, the improvements are more pronounced from BL (h = Neural, τ = 0.7) on ImageNet, corroborating our observations from Figure 3 in Section 3.1.

4 Adaptive Attacks Against SDMs

We now ask whether the robustness of even the reconfigured stateful defenses can be decreased with the introduction of better adaptive attacks. Specifically, we develop a family of attacks that aim to construct adversarial examples by *circumventing detection*.

4.1 Adjusting Attacks to Circumvent the Detection

As described in Section 2.5, traditional score-based black-box attacks such as NES [23, 41] and even hard-label attacks such as Boundary [6] iteratively operate in two stages. At a high-level, these attacks aim to (a) *estimate* the gradient or decision boundary, and (b) *move* in the direction of the gradient/boundary. For both stages, attacks submit several similar queries (e.g., both NES and Boundary query several copies of an image perturbed with Gaussian noise to estimate the gra-

Algorithm 1: NESRadialBinarySearch

Description: Binary search subroutine for finding optimal standard deviation that circumvents detection.

Input : Image x , SDM protecting model F

Output : Optimal query variance σ_{opt} for circumventing the SDM

Parameters: Standard deviation lower bound σ_{low} , upper bound σ_{high} , number of steps $steps$, number of samples $samples$, maximum action tolerance rate α

```
1  $\sigma_{opt} \leftarrow \sigma_{upper}$ 
2 for  $i = 1$  to  $steps$  do
3    $\sigma_{curr} \leftarrow (\sigma_{low} + \sigma_{high})/2$ 
4    $actions = 0$ 
5   for  $j = 1$  to  $samples$  do
6      $u \leftarrow \mathcal{N}(0, I)$ 
7      $x_g \leftarrow x + \sigma \cdot u$ 
8      $is\_action\_observed \leftarrow SDM(x_g)$ 
9     if  $is\_action\_observed$  then
10       $actions \leftarrow actions + 1$ 
11    if  $actions/samples \geq \alpha$  then
12       $\sigma_{lower} \leftarrow \sigma_{curr}$ 
13    else
14       $\sigma_{opt} \leftarrow \sigma_{curr}$ 
15       $\sigma_{upper} \leftarrow \sigma_{curr}$ 
16    end
17  end
18 end
```

dient and boundary respectively). However, SDMs operate by detecting and rejecting these similar queries. As such, these attacks do not succeed out-of-the-box against reconfigured SDMs, as evidenced by our results in Section 3.4. A successful attacker must therefore ensure that queries for both steps of the attack can circumvent detection.

Specifically, given an $SDM(f, h, d, Q, a, \tau, \text{action})$, for a query \mathbf{x} for either estimation or movement, the attacker seeks a parametric transformation T_θ (e.g., rotation of an image by θ degrees) such that $T_\theta(\mathbf{x})$ circumvents detection:

$$d(h(T_\theta(\mathbf{x}), c) \geq \tau \quad \forall c \in Q \quad (\text{circumvention})$$

while also yielding the necessary information:

$$F(T_\theta(\mathbf{x})) \approx F(\mathbf{x}) \quad (\text{utility})$$

By selecting a T_θ that satisfies these properties, the attacker has effectively queried \mathbf{x} without triggering the defense’s action.

4.1.1 Selecting a Transformation For Circumvention

Intuitively, one would like to select T_θ that distorts \mathbf{x} minimally to satisfy *utility*. On the other hand, T_θ must also be chosen to introduce sufficient distortion that satisfies *circumvention*, i.e., the attacker aims to find the T_θ that optimizes this tradeoff. To this end, we modify the estimation and movement steps of NES to obtain a new attack method, which we term as *NESRadial*, an adaptive score-based attack designed for stateful defenses. NESRadial adaptively transforms queries to significantly reduce robust accuracy for SDMs. Furthermore, we also implement similar modifications for Boundary to obtain *BoundaryRadial*, which are hard-label attack methods. We next introduce these two radial attack methods in more detail.

4.2 NESRadial: A Score-Based Attack

Recall from our discussion of traditional NES in Section 2.5 that its attack queries can be broadly classified into two groups: (1) gradient estimation queries (used to estimate the classifier

Algorithm 2: NESRadial Attack

Description: Our proposed NESRadial attack, which uses Algorithm 1 to find the optimal initial standard deviation that circumvents detection and adjusts it as necessary. Differences compared to vanilla NES highlighted in blue.

Input : Image \mathbf{x} , target label y , perturbation budget ϵ , SDM protecting model F

Output : Adversarial example \mathbf{x}^* where $\|\mathbf{x} - \mathbf{x}^*\| \leq \epsilon$

Parameters: Number of attack iterations n , step-size η , maximum tolerable consecutive actions β

```
1  $\mathbf{x}^* \leftarrow \mathbf{x}$ 
2 for  $i = 1$  to  $n$  do
3    $\sigma_{opt} \leftarrow \text{NESRadialBinarySearch}(\mathbf{x}, \text{SDM})$ 
4
5    $g \leftarrow \text{NESGradEstimate}(\sigma_{opt}, \epsilon)$ 
6    $\mathbf{x}^*, \text{action\_observed} \leftarrow \text{NESMove}(\mathbf{x}^*, g, \eta, \epsilon)$ 
7
8   if action_observed for last  $\beta$  steps then
9      $\eta = \eta/2$ 
10  if not action_observed for last  $\beta$  steps then
11     $\eta = \eta * 2$ 
12
13 end
14 return  $\mathbf{x}^*$ 
```

gradient as in Equation 3), and (2) gradient descent queries (used to perform gradient descent with the estimated gradient, as in Equation 4). We now describe how NESRadial (presented in Algorithm 2) adaptively transforms queries in both stages to circumvent the similarity checks.

Circumvention for gradient estimation. To estimate the gradient at image \mathbf{x} (as in Equation 3)), traditional NES adds fixed-variance Gaussian noise to \mathbf{x} and submits these queries to the defense (NESGradEstimate in Algorithm 2). To ensure that these queries circumvent detection, NESRadial additionally *adjusts the standard deviation σ of the added Gaussian perturbations* (which equivalently also adjusts the variance, σ^2). To find the minimal variance adjustment (as per Lemma 3.1), NESRadial employs a simple *binary-search protocol* by observing the stateful defense’s action. Binary-search ends when it identifies the smallest variance for which the action is no longer invoked, e.g., no rejection occurs. An overview of this protocol can be found in the subroutine *NESRadialBinarySearch* presented in Algorithm 1.

Circumvention for gradient descent. Given a gradient estimate, traditional NES descends by a fixed step-size in the direction of the gradient (NESMove in Algorithm 2). To ensure that these queries circumvent detection, our NESRadial algorithm, presented in 2, additionally *adjusts the step-size η of the gradient descent*. Specifically, NESRadial adaptively doubles the step-size when it observes multiple consecutive invocations of the defense action, e.g., multiple consecutive rejections, and halves the step-size when no actions are observed. It uses NESRadialBinarySearch as a subroutine to estimate the optimal standard deviation for the Gaussian distribution.

4.3 BoundaryRadial: A Hard-Label Attack

An SDM may choose to expose only the classifier’s output labels (f), and not label probabilities (F). In this case, the de facto strategy for an attacker is to use a hard-label attack like Boundary [6], which also operates in two stages: (a) boundary estimation queries, and (b) boundary movement queries. Such attacks typically start from an adversarial example of large perturbation, and move along the decision boundary towards the original image rather than the other way around (as in score-based attacks). As such, they present a novel challenge against SDMs, with regards to the sequence of queries submitted.

We first provide an overview of the original Boundary attack, and then present *BoundaryRadial* that, akin to NESRadial, adaptively transforms queries to circumvent detection.

Algorithm 3: BoundaryRadial Attack

Description: Our proposed BoundaryRadial attack, which adapts the magnitude of Gaussian samples for boundary walking circumvention and skips the second stage if the query is rejected. Differences compared to vanilla Boundary highlighted in blue.

Input : Image \mathbf{x} , target label y , perturbation budget ϵ , *SDM* protecting model f
Output : Adversarial example \mathbf{x}^* where $\|\mathbf{x} - \mathbf{x}^*\| \leq \epsilon$
Parameters: Number of attack iterations $steps$, boundary estimation variance δ , movement step-size η , action tolerance rate α , parameter adaptation rate γ

```

1  $\mathbf{x}^* \leftarrow \mathcal{U}(0, 255)$ 
2 for  $t = 1$  to  $steps$  do
3    $\mathbf{x}_{est}^* \leftarrow BoundaryEstimate(\mathbf{x}^*, \delta, \gamma)$ 
4
5   if  $action\_ct \geq \alpha$  then
6     |  $\delta \leftarrow \delta * \gamma$ 
7
8    $\mathbf{x}_{move}^t, action\_ct \leftarrow BoundaryMove(\mathbf{x}^*, \eta, \epsilon, \gamma)$ 
9
10  if  $action\_count == size(candidates)$  then
11    |  $\mathbf{x}^* = \text{best of } \mathbf{x}_{est}^t$ 
12  else
13    |  $\mathbf{x}^* = \text{best of } \mathbf{x}_{move}^t$ 
14  end
15
16 end

```

Boundary Overview. Boundary is a hard-label attack that starts from a randomly initialized adversarial image, e.g., from a uniform distribution $\mathcal{U}(0, 255)$ and then performs a “boundary walk” to reduce the size of the perturbation. Given image \mathbf{x} with true label y , Boundary iteratively operates in two stages.

First, the decision boundary at iteration t is estimated/walked by querying k samples from a Gaussian distribution as $u_i \sim \mathcal{N}(0, I)$:

$$\mathbf{x}_i^t = \mathbf{x}^{t-1} + u_i \quad \forall 1 \leq i \leq k \quad (14)$$

The magnitude of the sample u_i is scaled by a factor of $0 < \delta < 1$ from the magnitude of current perturbation $\|\mathbf{x}^{t-1} - \mathbf{x}\|$ as:

$$u_i = \delta \cdot \|\mathbf{x}^{t-1} - \mathbf{x}\| \cdot \frac{u_i}{\|u_i\|} \quad (15)$$

Non-adversarial samples obtained after this stage are discarded. Second, all remaining adversarial samples \mathbf{x}_i^t are moved with a step-size of η in the direction of original image \mathbf{x} :

$$\mathbf{x}_i^t = \mathbf{x}_i^t + \epsilon \cdot (\mathbf{x} - \mathbf{x}_i^t) \quad (16)$$

Again, all non-adversarial samples obtained after this stage are discarded, and the “best” one with the smallest perturbation distance is selected for the next iteration:

$$\mathbf{x}^t = \arg \min_{\mathbf{x}_i^t} \|\mathbf{x} - \mathbf{x}_i^t\| \quad (17)$$

This process is repeated until the ϵ constraint is met, i.e., $\|\mathbf{x}^t - \mathbf{x}\| \leq \epsilon$.

The two hyperparameters (δ and η) are dynamically adapted to adjust to the shape of the boundary. For the first stage, Boundary aims to have around a large fraction of Gaussian samples remain adversarial. To achieve this, Boundary adjusts the magnitude of the noise (δ) depending on the fraction of resulting queries that are adversarial — if it is too low (too many samples are non-adversarial), δ is increased, and vice-versa. If it is too high, then the samples are too big for fine-grained boundary walking and δ is reduced. For the second stage, the ϵ is similarly adjusted.

Dataset	Defense	Natural	NES	NESRadial
CIFAR10	BL ($h = \text{Pixel-SHA}$, $\tau = 0.7$)	91.6%	66.2% (5.3% / 0.2K)	10.0% (32.3% / 0.9K)
	BL ($h = \text{Neural}$, $\tau = 0.7$)	91.7%	56.8% (55.2% / 2.9K)	11% (37.1% / 0.9K)
ImageNet	BL ($h = \text{Pixel-SHA}$, $\tau = 0.7$)	78.1%	31.0% (0.7% / 1.9K)	8% (29.8% / 0.9K)
	BL ($h = \text{Neural}$, $\tau = 0.7$)	77.7%	67.0% (78.3% / 2.4K)	44% (49.6% / 0.5K)

Table 4: Accuracy, average attack collision rate, and average attack query count for NES and NESRadial against the reconfigured SDMs in Section 3.4. Lower accuracy implies the attack was more successful. For NES, we take the best attack from the three variances in Table 3 (column 4). We run NESRadial on images that NES was unable to attack (column 5). We find that NESRadial is effective at reducing robustness while also using fewer queries.

4.3.1 BoundaryRadial Design

An overview for BoundaryRadial is presented in Algorithm 3. At a high-level, it continues to operate in two stages (BoundaryEstimate and BoundaryMove in Algorithm 3), but makes two key changes:

Circumvention for boundary walking/estimation. Analogously to NESRadial’s adjustment of variance, BoundaryRadial adjusts the magnitude of the Gaussian samples u_i depending on the fraction of queries for which the defense action is invoked — if it is invoked too much, e.g., too many rejections, the variance is increased, and vice-versa. Essentially, queries for which the SDM responds with an action are treated as adversarial, which encourages δ to increase.

Circumvention for η descent. Given the adversarial samples from the first stage, vanilla Boundary then moves these samples with a step-size of η towards the original image \mathbf{x} . However, doing so may cause the action to be invoked. If this occurs and the query is rejected, BoundaryRadial simply sets \mathbf{x}^t to be the best result from the first stage (boundary estimation), i.e., “skips” the second stage.

5 Evaluating SDMs Against Radial Attacks

In this section, we present experimental results that aim to answer the following question — *are reconfigured SDMs robust even in the face of the adaptive NESRadial and BoundaryRadial attacks?* To answer this question, we begin by describing our experimental setup, followed by results.

5.1 Experimental Setup

We evaluate reconfigured SDMs BL ($h = \text{Pixel-SHA}$, $\tau = 0.7$) and BL ($h = \text{Neural}$, $\tau = 0.7$) against NESRadial and BoundaryRadial, as well as against standard NES and Boundary. For NES, we use the same attack configuration as described in Section 2. NESRadial employs the same configuration as NES, but additionally configures parameters for the binary search described in Algorithm 1, i.e., $\sigma_{low} = 0.001$ and $\sigma_{high} = 0.5$, $steps = 10$, $samples = 20$, and $\alpha = 0.1$. Both Boundary and BoundaryRadial are ℓ_2 attacks run under a normalized $\ell_2 = 0.05$ bound, calculated as $\sqrt{\frac{1}{|\mathbf{x}|} \sum_{i=0}^{|\mathbf{x}|} (\mathbf{x}_{adv} - \mathbf{x})^2} = 0.05$ as per prior work [11, 27]. For Boundary and BoundaryRadial (which share the same set of parameters), we configure the parameters described in Algorithm 3 using the default values from the popular IBM ART framework [32], i.e., $steps = 1000$ (equivalent to a budget of 40k queries), $\delta = 0.01$, $\eta = 0.01$, $\alpha = 0.80$, and $\gamma = 0.667$. All attacks are run until either success, or budget is exhausted.

5.2 Results

Table 4 presents the accuracy under the score-based NES (column 4) and NESRadial (column 5) attacks. For all SDMs and datasets, NESRadial is able to significantly further reduce robust accuracy. For CIFAR10, NESRadial is able to reduce both SDMs to effectively random classifiers. On ImageNet, BL($h = \text{Pixel-SHA}$, $\tau = 0.7$) drops as low as 8%. Interestingly, BL($h = \text{Neural}$, $\tau = 0.7$) is also considerably more robust on ImageNet with a 44% accuracy, once again corroborating the hypothesis from Section 3.1 that contrastively-trained neural extractors may be significantly more effective on higher-dimensional images. Finally, we also find that NESRadial can potentially reduce

Dataset	Defense	Natural	Boundary	BoundaryRadial
CIFAR10	BL ($h = \text{Pixel-SHA}$, $\tau = 0.7$)	91.6%	91.0% (99.8% / 1.0K)	0.0% (43.6% / 3.1K)
	BL ($h = \text{Neural}$, $\tau = 0.7$)	91.7%	23.8% (60.8% / 1.7K)	12.4% (76.3% / 1.0K)
ImageNet	BL ($h = \text{Pixel-SHA}$, $\tau = 0.7$)	78.1%	76.0% (57.6% / 0.8K)	30.0% (18.9% / 6.2K)
	BL ($h = \text{Neural}$, $\tau = 0.7$)	77.7%	62.0% (89.3% / 30.7K)	55.0% (92.3% / 1.3K)

Table 5: Accuracy, average attack collision rate, and average attack query count for Boundary and BoundaryRadial against the reconfigured SDMs in Section 3.4. Lower accuracy implies the attack was more successful. We run BoundaryRadial on images that Boundary was unable to attack (column 5). We find that BoundaryRadial is effective at reducing robustness while also using fewer queries in some cases.

Dataset	Defense	Natural	NESRadial	BoundaryRadial
CIFAR10	BL ($h = \text{AHash}$, $\tau = 0.7$)	91.7%	5.4% (14.1% / 0.6K)	14.2% (62.2% / 1.0K)
	BL ($h = \text{PHash}$, $\tau = 0.7$)	91.7%	5.6% (19.7% / 0.6K)	14.2% (60.7% / 1.1K)
	BL ($h = \text{WaveletHash}$, $\tau = 0.7$)	91.7%	4.4% (14.0% / 0.6K)	14.8% (63.7% / 1.1K)

Table 6: Accuracy, average attack collision rate, and average attack query count for NESRadial and BoundaryRadial against the ablative SDMs in Section 5.3 with different hash functions as feature extractors. Lower accuracy implies the attack was more successful. We find that NESRadial and BoundaryRadial are effective attacks against these hash functions.

the query count, demonstrating reductions of upto $\sim 5x$ the query cost when compared to standard NES.

Table 5 similarly presents accuracy under hard-label Boundary (column 4) and BoundaryRadial (column 5) attacks. Despite the hard-label setting, BoundaryRadial is able to drop robust accuracy of $BL(h = \text{Pixel-SHA}, \tau = 0.7)$ to 0% on CIFAR10, in comparison to the 91% of the barely successful vanilla Boundary (natural accuracy is 91.6%). BoundaryRadial also exhibits similar trends for ImageNet, and reductions of upto $\sim 23\times$ the query cost in some cases (e.g., with BoundaryRadial versus Boundary for $BL(h = \text{Neural}, \tau = 0.7)$).

5.3 Alternative Configurations

The framework presented in Section 2 allows for a number of new potential SDM configurations. While the majority of this work focused on understanding and evaluating existing SDMS (and their principled reconfigurations), we now consider alternative configurations. Specifically, there exists a vast body of work on perceptual feature extraction, outside the realm of adversarial defense [16]. Given that NESRadial and BoundaryRadial were able to significant reduce the robust accuracy for Pixel-SHA and neural extractor-based SDMS, a natural question arises — would other feature extractors work better?

We provide preliminary insight into answering this question by evaluating the robust accuracy of SDM configurations with three popular perceptual feature extractors: PHash (DCT-based), AHash (AES-based), and WaveletHash (DWT-based). Results can be found in Table 6 — *these hash functions do not provide any gains in robustness*. In fact, their accuracies are significantly lower than the reconfigurations discussed in Section 3.4, and used throughout this work. We find that this can be explained by evaluating the detection rate and natural accuracy (failure modes for Pixel-SHA and neural extractors defenses from Section 3) for these functions. Once again, practical choices for threshold τ (Figure 5) are limited to values for which detection rate drops significantly over larger attack query variance (Figure 4).

6 Related Work

6.1 Query-Based Black-Box Attacks

Query-based black-box attacks such as NES [23] and Boundary [6] aim to construct an adversarial example without access to model parameters and architecture, i.e., without access to gradients.

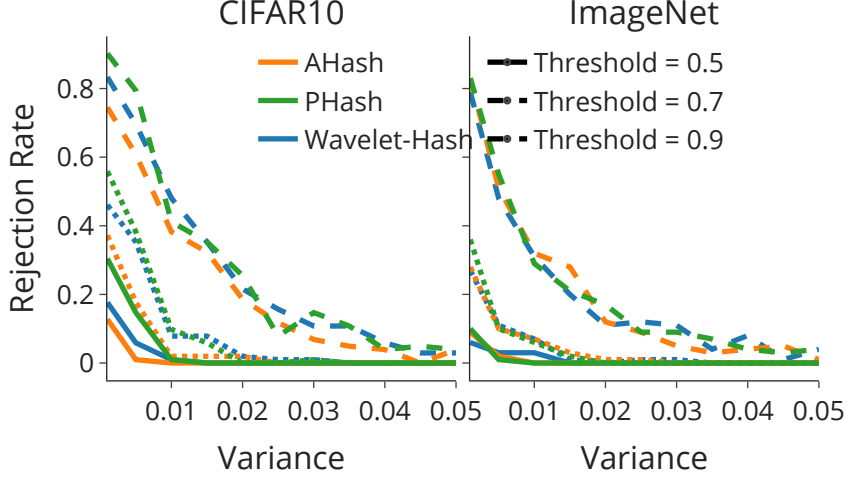


Figure 4: Detection rate vs. attack query variance for alternative feature extractors: pHash, aHash, and WaveletHash.

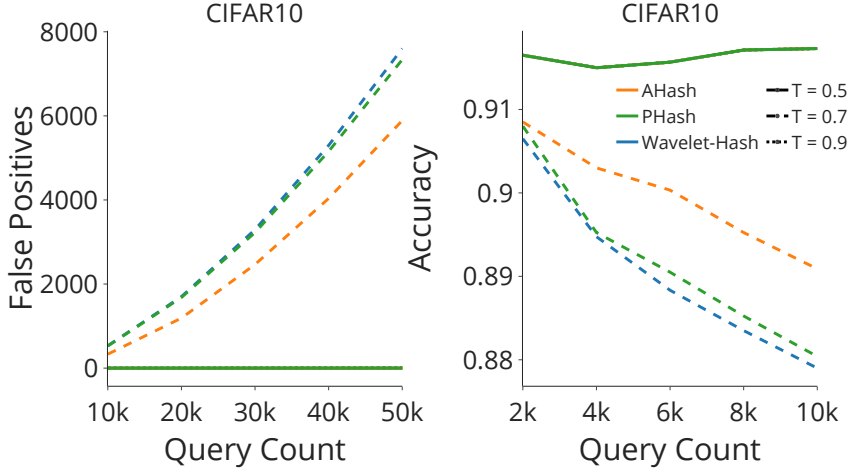


Figure 5: False positive rate vs. query count for alternative feature extractors: pHash, aHash, and WaveletHash.

Attacks can be categorized into score-based (when label probabilities are available), and hard-label (when only labels are available). Since the attacker only has access to model outputs, these attacks instead proceed via techniques adapted from the black-box optimization literature. Such approaches typically aim to estimate gradients through localized differences or some proxy and include attacks such as OPT [12], HopSkipJumpAttack [9], QEBA [26], POLICY [42], SurFree [30], and ECO [31].

In this work, we focus on NES [23] and Boundary [6] as well performing soft-label and hard-label attacks respectively and extend these attacks to NESRadial and BoundaryRadial, which makes adaptations to avoid SDM collisions.

Other Types of Black-Box Attacks. The alternative to query-based attacks is the *transfer attack*, which proceeds by training a local substitute model on the same classification task as the target classifier, and constructing white-box adversarial examples against this substitute in the hopes that they will transfer to the target classifier. While these attacks are considerably weaker than direct query-based approaches [23], strong substitute models can be created by techniques such as model stealing [24]. We follow prior work on stateful defenses and consider defending against transfer at-

tacks to be an orthogonal problem — transfer attack defenses already exist [39] and can be combined with stateful systems to build a more complete defense.

6.1.1 Query Blinding

Chen et al. [11] proposed query blinding attacks as an adaptive attack against OSD. Specifically, this attack aims to evade OSD’s rejection system by applying transformations such as rotation, lighting, translation, etc. to evade the query detection system. The goal of this approach is to make transformed queries that are do not collide with prior queries but are still useful for estimating gradients.

Query blinding is orthogonal and complementary to NESRadial and BoundaryRadial. Specifically, query blinding could be combined with NESRadial or BoundaryRadial. The usage of Gaussian noise tuning in NESRadial can also be generalized to other transforms.

6.2 Detecting Black-Box Attacks

In this paper, we consider SDM models that detect similar queries that may be indicative of a black-box adversarial attack. Specifically, we considered OSD [11] and Blacklight [27] as described in Section 2.4.

Other approaches to detecting black-box attacks include Adversarial Attack on Attackers (AAA) [10] and AdvMind [33]. AAA is a post-processing attack that attempts to modify the logits loss curve to locally point in the incorrect attack direction in a periodic fashion, misguiding score-based query attacks from a successful attack. AdvMind proposes a detection model that aims to infer the intent of an adversary and detect attacks. While these approaches both aim to thwart black-box attacks, they are orthogonal to the SDMs we focus on that aim to detect similar queries.

7 Conclusion

In conclusion, we found that SDMs, in particular Blacklight [27], were less robust than had been previously thought. Motivated by this finding, we provide a systematization of stateful defenses and analyze when SDM models may or may not work well. Using the general framework, we identify potential limitations of such defenses. Motivated by this analysis, we propose a new class of attacks with NESRadial and BoundaryRadial, which we find to be very effective in reducing the robustness of SDMs. We thus suggest that future stateful defenses should be evaluated against NESRadial and BoundaryRadial.

References

- [1] Automatic license plate recognition - high accuracy alpr, Oct 2022.
- [2] Amazon. Amazon rekognition: Automate your image recognition and video analysis with machine learning.
- [3] Anish Athalye, Nicholas Carlini, and David Wagner. Obfuscated gradients give a false sense of security: Circumventing defenses to adversarial examples. In *International conference on machine learning*, pages 274–283. PMLR, 2018.
- [4] Sean Bell and Kavita Bala. Learning visual similarity for product design with convolutional neural networks. *ACM transactions on graphics (TOG)*, 34(4):1–10, 2015.
- [5] Russell Brandom and Richard Lawler. Apple reveals new efforts to fight child abuse imagery, Aug 2021.
- [6] Wieland Brendel, Jonas Rauber, and Matthias Bethge. Decision-based adversarial attacks: Reliable attacks against black-box machine learning models. *arXiv preprint arXiv:1712.04248*, 2017.
- [7] Tom B Brown, Dandelion Mané, Aurko Roy, Martín Abadi, and Justin Gilmer. Adversarial patch. *arXiv preprint arXiv:1712.09665*, 2017.

- [8] Casey Chan. What facebook deals with everyday: 2.7 billion likes, 300 million photos uploaded and 500 terabytes of data, Aug 2012.
- [9] Jianbo Chen, Michael I Jordan, and Martin J Wainwright. Hopskipjumpattack: A query-efficient decision-based attack. In *2020 ieee symposium on security and privacy (sp)*, pages 1277–1294. IEEE, 2020.
- [10] Sizhe Chen, Zhehao Huang, Qinghua Tao, Yingwen Wu, Cihang Xie, and Xiaolin Huang. Adversarial attack on attackers: Post-process to mitigate black-box score-based query attacks. *arXiv preprint arXiv:2205.12134*, 2022.
- [11] Steven Chen, Nicholas Carlini, and David Wagner. Stateful detection of black-box adversarial attacks. In *Proceedings of the 1st ACM Workshop on Security and Privacy on Artificial Intelligence*, pages 30–39, 2020.
- [12] Minhao Cheng, Thong Le, Pin-Yu Chen, Jinfeng Yi, Huan Zhang, and Cho-Jui Hsieh. Query-efficient hard-label black-box attack: An optimization-based approach. *arXiv preprint arXiv:1807.04457*, 2018.
- [13] Clarifai. The world’s ai: Clarifai computer vision ai and machine learning platform.
- [14] Francesco Croce and Matthias Hein. Reliable evaluation of adversarial robustness with an ensemble of diverse parameter-free attacks. In *International conference on machine learning*, pages 2206–2216. PMLR, 2020.
- [15] John R Douceur. The sybil attack. In *Peer-to-Peer Systems: First International Workshop, IPTPS 2002 Cambridge, MA, USA, March 7–8, 2002 Revised Papers 1*, pages 251–260. Springer, 2002.
- [16] Ling Du, Anthony TS Ho, and Runmin Cong. Perceptual hashing for image authentication: A survey. *Signal Processing: Image Communication*, 81:115713, 2020.
- [17] Kevin Eykholt, Ivan Evtimov, Earlene Fernandes, Bo Li, Amir Rahmati, Chaowei Xiao, Atul Prakash, Tadayoshi Kohno, and Dawn Song. Robust physical-world attacks on deep learning visual classification. In *Proceedings of the IEEE conference on computer vision and pattern recognition*, pages 1625–1634, 2018.
- [18] Ryan Feng, Neal Mangaokar, Jiefeng Chen, Earlene Fernandes, Somesh Jha, and Atul Prakash. Graphite: Generating automatic physical examples for machine-learning attacks on computer vision systems. In *2022 IEEE 7th European Symposium on Security and Privacy (EuroS&P)*, pages 664–683. IEEE, 2022.
- [19] Andreas Geiger, Philip Lenz, and Raquel Urtasun. Are we ready for autonomous driving? the kitti vision benchmark suite. In *2012 IEEE conference on computer vision and pattern recognition*, pages 3354–3361. IEEE, 2012.
- [20] Ian J Goodfellow, Jonathon Shlens, and Christian Szegedy. Explaining and harnessing adversarial examples. *arXiv preprint arXiv:1412.6572*, 2014.
- [21] Varun Gulshan, Lily Peng, Marc Coram, Martin C Stumpe, Derek Wu, Arunachalam Narayanaswamy, Subhashini Venugopalan, Kasumi Widner, Tom Madams, Jorge Cuadros, et al. Development and validation of a deep learning algorithm for detection of diabetic retinopathy in retinal fundus photographs. *Jama*, 316(22):2402–2410, 2016.
- [22] Kaiming He, Xiangyu Zhang, Shaoqing Ren, and Jian Sun. Deep residual learning for image recognition. In *Proceedings of the IEEE conference on computer vision and pattern recognition*, pages 770–778, 2016.
- [23] Andrew Ilyas, Logan Engstrom, Anish Athalye, and Jessy Lin. Black-box adversarial attacks with limited queries and information. In *International conference on machine learning*, pages 2137–2146. PMLR, 2018.
- [24] Mika Juuti, Sebastian Szyller, Samuel Marchal, and N Asokan. Prada: protecting against dnn model stealing attacks. In *2019 IEEE European Symposium on Security and Privacy (EuroS&P)*, pages 512–527. IEEE, 2019.

[25] Alex Krizhevsky, Geoffrey Hinton, et al. Learning multiple layers of features from tiny images. 2009.

[26] Huchen Li, Xiaojun Xu, Xiaolu Zhang, Shuang Yang, and Bo Li. Qeba: Query-efficient boundary-based blackbox attack. In *Proceedings of the IEEE/CVF conference on computer vision and pattern recognition*, pages 1221–1230, 2020.

[27] Huiying Li, Shawn Shan, Emily Wenger, Jiayun Zhang, Haitao Zheng, and Ben Y Zhao. Black-light: Scalable defense for neural networks against {Query-Based}{Black-Box} attacks. In *31st USENIX Security Symposium (USENIX Security 22)*, pages 2117–2134, 2022.

[28] Nathan Linial. Finite metric spaces: Combinatorics, geometry and algorithms. In *Proceedings of the Eighteenth Annual Symposium on Computational Geometry*, SCG ’02, page 63, New York, NY, USA, 2002. Association for Computing Machinery.

[29] Aleksander Madry, Aleksandar Makelov, Ludwig Schmidt, Dimitris Tsipras, and Adrian Vladu. Towards deep learning models resistant to adversarial attacks. *arXiv preprint arXiv:1706.06083*, 2017.

[30] Thibault Maho, Teddy Furon, and Erwan Le Merrer. Surfree: a fast surrogate-free black-box attack. In *Proceedings of the IEEE/CVF Conference on Computer Vision and Pattern Recognition*, pages 10430–10439, 2021.

[31] Seungyong Moon, Gaon An, and Hyun Oh Song. Parsimonious black-box adversarial attacks via efficient combinatorial optimization. In *International Conference on Machine Learning*, pages 4636–4645. PMLR, 2019.

[32] Maria-Irina Nicolae, Mathieu Sinn, Minh Ngoc Tran, Beat Buesser, Ambrish Rawat, Martin Wistuba, Valentina Zantedeschi, Nathalie Baracaldo, Bryant Chen, Heiko Ludwig, Ian Molloy, and Ben Edwards. Adversarial robustness toolbox v1.2.0. *CoRR*, 1807.01069, 2018.

[33] Ren Pang, Xinyang Zhang, Shouling Ji, Xiapu Luo, and Ting Wang. Advmind: Inferring adversary intent of black-box attacks. In *Proceedings of the 26th ACM SIGKDD International Conference on Knowledge Discovery & Data Mining*, pages 1899–1907, 2020.

[34] Jiameng Pu, Neal Mangaokar, Lauren Kelly, Parantapa Bhattacharya, Kavya Sundaram, Mobin Javed, Bolun Wang, and Bimal Viswanath. Deepfake videos in the wild: Analysis and detection. In *Proceedings of the Web Conference 2021*, pages 981–992, 2021.

[35] Olga Russakovsky, Jia Deng, Hao Su, Jonathan Krause, Sanjeev Satheesh, Sean Ma, Zhiheng Huang, Andrej Karpathy, Aditya Khosla, Michael Bernstein, et al. Imagenet large scale visual recognition challenge. *International journal of computer vision*, 115:211–252, 2015.

[36] Thalles Santos Silva. Exploring simclr: A simple framework for contrastive learning of visual representations. <https://sthalles.github.io>, 2020.

[37] Yi Sun, Xiaogang Wang, and Xiaou Tang. Deep learning face representation from predicting 10,000 classes. In *Proceedings of the IEEE conference on computer vision and pattern recognition*, pages 1891–1898, 2014.

[38] Florian Tramer, Nicholas Carlini, Wieland Brendel, and Aleksander Madry. On adaptive attacks to adversarial example defenses. *Advances in neural information processing systems*, 33:1633–1645, 2020.

[39] Florian Tramèr, Alexey Kurakin, Nicolas Papernot, Ian Goodfellow, Dan Boneh, and Patrick McDaniel. Ensemble adversarial training: Attacks and defenses. *arXiv preprint arXiv:1705.07204*, 2017.

[40] Dayong Wang, Aditya Khosla, Rishab Gargya, Humayun Irshad, and Andrew H Beck. Deep learning for identifying metastatic breast cancer. *arXiv preprint arXiv:1606.05718*, 2016.

[41] Daan Wierstra, Tom Schaul, Tobias Glasmachers, Yi Sun, Jan Peters, and Jürgen Schmidhuber. Natural evolution strategies. *The Journal of Machine Learning Research*, 15(1):949–980, 2014.

[42] Ziang Yan, Yiwen Guo, Jian Liang, and Changshui Zhang. Policy-driven attack: learning to query for hard-label black-box adversarial examples. In *International Conference on Learning Representations*, 2021.

[43] Zhi Yang, Christo Wilson, Xiao Wang, Tingting Gao, Ben Y Zhao, and Yafei Dai. Uncovering social network sybils in the wild. *ACM Transactions on Knowledge Discovery from Data (TKDD)*, 8(1):1–29, 2014.

A NES using Non Standard Variance

Lemma A.1. *1. Concentration of measure for Gaussians* Let G be a $k \times d$ random matrix with rows $\sigma g^i \sim \mathcal{N}(0, \sigma^2) \forall 1 \leq i \leq k$. Then, for any unit vector $v \in \mathbb{R}^d$,

$$P[|\|Gv\|^2 - 1| > \epsilon] \leq 2 \exp\left(-\left(k + \frac{\epsilon + 1}{2\sigma^2}\right)\right)$$

Proof. Note that by rotational invariance of Gaussians, $Gv \stackrel{D}{=} Ge^1$, where e^1 is the standard basis vector. This implies that $\|Gv\|^2 \stackrel{D}{=} \|Ge^1\|^2 \stackrel{D}{=} \sigma^2 \chi_k^2$, where χ_k^2 is a chi-square random variable with k -degrees of freedom. Then, by Chernoff's bounding method:

$$\begin{aligned} P[|\|Gv\|^2 - 1| > \epsilon] &= P[|\sigma^2 \chi_k^2 - 1| > \epsilon] \\ &\leq 2 \inf_{t>0} e^{-\epsilon t} \mathbb{E}[e^{t(\sigma^2 \chi_k^2 - 1)}] \\ &\leq 2 \inf_{t>0} e^{-\epsilon t - t} \mathbb{E}[e^{t\sigma^2 \chi_k^2}] \\ &\leq 2 \inf_{t>0} e^{-\epsilon t - t} (1 - 2\sigma^2 t)^{-\frac{k}{2}} \\ &\leq 2 \inf_{t>0} e^{-\epsilon t - t - \frac{k}{2} \log(1 - 2\sigma^2 t)} \\ &\leq 2e^{-\frac{\epsilon - k\sigma^2 + 1}{2\sigma^2} - \frac{k}{2} \log(\frac{\sigma^2}{\epsilon + 1})} \\ &\leq 2e^{-\frac{(\epsilon + 1 - \sigma^2 k)^2}{2\sigma^2(1 + \epsilon)}} \\ &\leq 2e^{-\frac{(\epsilon + 1)^2 - 2\sigma^2 k(\epsilon + 1)}{2\sigma^2(1 + \epsilon)}} \\ &\leq 2e^{-\frac{\epsilon + 1 - 2\sigma^2 k}{2\sigma^2}} \\ &\leq 2e^{-k} e^{-\frac{\epsilon + 1}{2\sigma^2}} \\ &\leq 2e^{-k - \frac{\epsilon + 1}{2\sigma^2}} \end{aligned}$$

□

A.0.1 Proof for Theorem 3.1

Let $\mathbf{x} \in \mathbf{R}^d$ be an image query, ∇_x be the true gradient for classifier loss L , and $g_1, \dots, g_k \in \mathbf{R}^d$ be k Gaussian vectors of variance σ^2 . Then, the norm of estimated gradient $G \cdot \nabla_x$ (where G is a matrix of rows g_1, \dots, g_k) is bounded in probability by:

$$\begin{aligned} P[(1 - \delta)\|\nabla_x\| \leq \|G \cdot \nabla_x\| \leq (1 + \delta)\|\nabla_x\|] &\geq \\ 1 - 2 \cdot \exp\left(-k - \frac{1 + \delta}{2\sigma^2}\right) \end{aligned}$$

where $0 \leq \delta \leq 1$ is the estimation error.

Proof.

$$\begin{aligned}
& P[(1 - \delta)\|\nabla_x\| \leq \|G\nabla_x\| \leq (1 + \delta)\|\nabla_x\|] \\
&= P[(1 - \delta)^2\|\nabla_x\|^2 \leq \|G\nabla_x\|^2 \leq (1 + \delta)^2\|\nabla_x\|^2] \\
&\geq P\left[1 - \delta \leq \frac{\|G\nabla_x\|^2}{\|\nabla_x\|^2} \leq 1 + \delta\right] \\
&= P\left[\left|\frac{\|G\nabla_x\|^2}{\|\nabla_x\|^2} - 1\right| \leq \delta\right] \\
&= P\left[\left|\left\|G\frac{\nabla_x}{\|\nabla_x\|}\right\|^2 - 1\right| \leq \delta\right] \\
&\geq 1 - 2e^{-k - \frac{\delta+1}{2\sigma^2}}
\end{aligned}$$

Where the last step is by Lemma 1. \square

B Trade-off between Attack Detection and False Positives

Lemma B.1. For a n -dimensional gaussian random vector $\mathbf{u} \sim \mathcal{N}(0, \sigma^2)$ and $\frac{b}{\sigma} < 1$,

$$\mathbb{P}_{\mathbf{u} \sim \mathcal{N}(0, \sigma^2)}[\|\mathbf{u}\|_2 \leq \sqrt{nb}] \leq e^{\frac{n}{2}} \frac{b^n}{\sigma^n} \quad (18)$$

Proof. We can also write the LHS as

$$\mathbb{P}_{\mathbf{u} \sim \mathcal{N}(0, \sigma^2)}\left[\left\|\frac{\mathbf{u}}{\sigma}\right\|_2^2 \leq \frac{nb^2}{\sigma^2}\right] \quad (19)$$

Now, for $t < 0$,

$$\mathbb{P}_{\mathbf{u} \sim \mathcal{N}(0, \sigma^2)}\left[\left\|\frac{\mathbf{u}}{\sigma}\right\|_2^2 \leq \frac{nb^2}{\sigma^2}\right] = \mathbb{P}_{\mathbf{u} \sim \mathcal{N}(0, \sigma^2)}\left[e^{t\left\|\frac{\mathbf{u}}{\sigma}\right\|_2^2} \geq e^{t\frac{nb^2}{\sigma^2}}\right] \quad (20)$$

Applying Markov's inequality ($\mathbb{P}[X \geq a] \leq \frac{\mathbb{E}[X]}{a}$), we get

$$\mathbb{P}_{\mathbf{u} \sim \mathcal{N}(0, \sigma^2)}\left[e^{t\left\|\frac{\mathbf{u}}{\sigma}\right\|_2^2} \geq e^{t\frac{nb^2}{\sigma^2}}\right] \leq \frac{\mathbb{E}\left[e^{t\left\|\frac{\mathbf{u}}{\sigma}\right\|_2^2}\right]}{e^{t\frac{nb^2}{\sigma^2}}} \quad (21)$$

If $\mathbf{u} \sim \mathcal{N}(0, \sigma^2)$, then $\frac{\mathbf{u}}{\sigma} \sim \mathcal{N}(0, 1)$. And $\frac{\|\mathbf{u}\|_2^2}{\sigma^2} \sim \mathcal{X}_n^2$ follows the chi-square distribution. Using the moment generating function for chi-square distribution in Eq. 21 and combining with Eq. 20, we get

$$\begin{aligned}
\mathbb{P}_{\mathbf{u} \sim \mathcal{N}(0, \sigma^2)}\left[\left\|\frac{\mathbf{u}}{\sigma}\right\|_2^2 \leq \frac{nb^2}{\sigma^2}\right] &\leq \frac{(1 - 2t)^{-\frac{n}{2}}}{e^{t\frac{nb^2}{\sigma^2}}} \\
&= \exp\left(\frac{-n}{2} \log(1 - 2t) - \frac{tnb^2}{\sigma^2}\right)
\end{aligned} \quad (22)$$

To get a tight upper bound, we can replace a value of t that minimizes the RHS i.e. $t = \frac{1}{2}\left[1 - \frac{\sigma^2}{b^2}\right]$. Since, $t < 0$, we need $\sigma > b$. Using this, we get

$$\begin{aligned}
\mathbb{P}_{\mathbf{u} \sim \mathcal{N}(0, \sigma^2)}\left[\left\|\frac{\mathbf{u}}{\sigma}\right\|_2^2 \leq \frac{nb^2}{\sigma^2}\right] &\leq \exp\left(\frac{n}{2} \log\left(\frac{b^2}{\sigma^2}\right) - \frac{nb^2}{2\sigma^2} + \frac{n}{2}\right) \\
&\leq \exp\left(\frac{n}{2} \log\left(\frac{b^2}{\sigma^2}\right) + \frac{n}{2}\right) \\
&= e^{\frac{n}{2}} \frac{b^n}{\sigma^n}
\end{aligned} \quad (23)$$

\square

Given $SDM(f, h, d, Q, a, \tau, \text{action})$ for data distribution \mathcal{D} , consider $h : \mathcal{X} \rightarrow \mathcal{H}$ to be a feature extractor that maps from the metric space $(\mathcal{X}, \hat{\ell}_2)$ to (\mathcal{H}, d) . Here, (1) the n -dimensional input space $\mathcal{X} \in [0, 1]^n$, (2) $\hat{\ell}_2$ is the normalized euclidean distance and, (3) $d : \mathcal{H} \times \mathcal{H} \rightarrow [0, 1]$ is a distance metric defined on the hash space. From previous work in metric spaces [28], we define the expansion and contraction properties of h to be:

$$\text{expansion}(h) : E_h = \max_{\mathbf{x}, \mathbf{y} \in \mathcal{X}} \frac{d(h(\mathbf{x}), h(\mathbf{y}))}{\frac{\|\mathbf{x} - \mathbf{y}\|_2}{\sqrt{n}}} \quad (24)$$

$$\text{contraction}(h) : C_h = \max_{\mathbf{x}, \mathbf{y} \in \mathcal{X}} \frac{\frac{\|\mathbf{x} - \mathbf{y}\|_2}{\sqrt{n}}}{d(h(\mathbf{x}), h(\mathbf{y}))} \quad (25)$$

We redefine the attack detection and false positive rates over the marginal data distribution $\mathcal{D}_{\mathcal{X}}$ as

$$\alpha^{det} = \mathbb{P}_{\mathbf{x} \sim \mathcal{D}_{\mathcal{X}}, \mathbf{u} \sim \mathcal{N}(0, \sigma^2)} [d(h(\mathbf{x} + \mathbf{u}), h(\mathbf{x})) < \tau] \quad (26)$$

$$\alpha^{fp} = \mathbb{P}_{\mathbf{v}, \mathbf{x} \sim \mathcal{D}_{\mathcal{X}}} [d(h(\mathbf{v}), h(\mathbf{x})) < \tau] \quad (27)$$

Theorem B.2. *Given the above setting, an $SDM(f, h, d, Q, a, \tau, \text{action})$ cannot improve both - increase the attack detection rate (α^{det}) and decrease the false positive rate (α^{fp}). This trade-off is upper bounded by the expansion (E_h) and contraction (C_h) of the feature extractor, and the average normalized ℓ_2 distance between images in the marginal input distribution $\mathcal{D}_{\mathcal{X}}$, given by :*

$$\alpha^{det} (1 - n\alpha^{fp}) \leq \left(\frac{\sqrt{e}}{\sqrt{n}} \frac{M_{\mathcal{D}_{\mathcal{X}}} E_h C_h}{\sigma} \right)^n \quad (28)$$

where, $M_{\mathcal{D}_{\mathcal{X}}} = \mathbb{E}_{\mathbf{v}, \mathbf{x} \sim \mathcal{D}_{\mathcal{X}}} [\|\mathbf{v} - \mathbf{x}\|_2]$.

Proof. Using Eq. 25 in Eq. 26, we get

$$\alpha^{det} \leq \mathbb{P}_{\mathbf{u} \sim \mathcal{N}(0, \sigma^2)} [\|\mathbf{u}\|_2 < \sqrt{n} C_h \tau] \quad (29)$$

Similarly, using Eq. 24 in Eq. 27, we get

$$\alpha^{fp} \geq \mathbb{P}_{\mathbf{v}, \mathbf{x} \sim \mathcal{D}_{\mathcal{X}}} [\|\mathbf{v} - \mathbf{x}\|_2 < \frac{\sqrt{n} \tau}{E_h}] \quad (30)$$

Now, applying lemma B.1 in Eq. 29 with $b = C_h \tau$, we get

$$\alpha^{det} \leq e^{\frac{n}{2}} \frac{C_h^n \tau^n}{\sigma^n} \quad (31)$$

Now, we can rewrite Eq 30 as

$$\alpha^{fp} \geq 1 - \mathbb{P}_{\mathbf{v}, \mathbf{x} \sim \mathcal{D}_{\mathcal{X}}} [\|\mathbf{v} - \mathbf{x}\|_2 \geq \frac{\sqrt{n} \tau}{E_h}] \quad (32)$$

Applying markov's inequality in Eq. 32, we get

$$\alpha^{fp} \geq 1 - \frac{E_h}{\sqrt{n} \tau} \mathbb{E}_{\mathbf{v}, \mathbf{x} \sim \mathcal{D}_{\mathcal{X}}} [\|\mathbf{v} - \mathbf{x}\|_2] \quad (33)$$

Rearranging and substituting $M_{\mathcal{D}_{\mathcal{X}}} = \frac{1}{\sqrt{n}} \mathbb{E}_{\mathbf{v}, \mathbf{x} \sim \mathcal{D}_{\mathcal{X}}} [\|\mathbf{v} - \mathbf{x}\|_2]$, we get

$$\tau \leq \frac{E_h M_{\mathcal{D}_{\mathcal{X}}}}{1 - \alpha^{fp}} \quad (34)$$

Now, using Eq. 34 in Eq. 31, we get

$$\begin{aligned} \alpha^{det} &\leq e^{\frac{n}{2}} \frac{E_h^n C_h^n}{\sigma^n} \frac{M_{\mathcal{D}_{\mathcal{X}}}}{(1 - \alpha^{fp})^n} \\ &\leq e^{\frac{n}{2}} \frac{E_h^n C_h^n}{\sigma^n} \frac{M_{\mathcal{D}_{\mathcal{X}}}}{(1 - n\alpha^{fp})} \end{aligned} \quad (35)$$

By rearranging, we finally get

$$\alpha^{det}(1 - n\alpha^{fp}) \leq e^{\frac{n}{2}} \frac{C_h^n E_h^n M_{\mathcal{D}_{\mathcal{X}}}^n}{\sigma^n} \quad (36)$$

□